T1-T2 WEIGHTED MR IMAGE COMPOSITION AND CATALOGUING OF BRAIN TUMOR USING REGULARIZED LOGISTIC REGRESSION
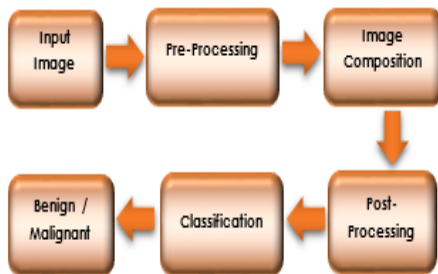
D. Aju*, R. Rajkumar

School of Computing Science and Engineering, VIT University, Vellore, Tamil Nadu, India

*Corresponding author
daju@vit.ac.in

Graphical abstract

Abstract

In medical diagnosis, the functional and structural information of the brain as well as the impending abnormal tissues is very crucial and important with an MR image. A collective CAD system that detects and classifies the brain tumor by exploiting the structural information is presented. Magnetic Resonance Imaging (MRI) T1-weighted and T2-weighted images provides suitable variation of contrast between the different soft tissues of the brain which is suitable for detecting the brain tumor. Both the Magnetic Resonance (MR) image sequences are composited using the alpha blending technique. The tumor area in the MR images will be segmented using the Enhanced Watershed Segmentation (EWATS) algorithm. The feature extraction is a means of signifying the raw image data in its abridged form to ease the classification in a better way. An expert classification assistant is tried out to help the physicians to classify the detected MRI brain tumor in an efficient manner. The proposed method uses the Regularized Logistic Regression (RLR) for the efficient cataloguing of brain tumor in which it achieves an effective accuracy rate of 96%, specificity rate of 86% and sensitivity rate of 97%.

Keywords: Brain Tumor, Alpha Blending, EWATS, GLCM, RLR, Cataloguing

1.0 INTRODUCTION

The definitive purpose of a brain tumor imaging analysis is to extract the diagnostic features and the patient-specific significant clinical data [18] from the scanned MR images and cataloguing it accordingly. Cataloguing refers to the classification of brain tumor into different category. Attaining higher spatial resolution and the capability of discriminating the brain soft tissues in a better way is the advantage of MR imaging. With no repositioning of the patients, images of the brain can be acquired in multiple planes such as axial, sagittal, coronal, and oblique.

A single MR image sequence is not adequate to segment and isolate the tumor affected area due to character and appearance [7] of brain tumors. In therapeutic practices, different MRI sequences are utilized for the diagnosis and prognosis of the tumor. Basically, the sequences include T1-weighted and T2-weighted MR images. The commonly used image sequence is the T1-weighted where it helps the physicians to annotate the healthy tissues easily. The tumor border area can be made brighter by increasing the contrast of the image whereby the tumor area and the necrotic region can be differentiated clearly. The edema region surrounding the tumor looks bright in T2-weighted MR images. Both these image sequences can be blended together to obtain an improved image for further processing.

In MR images, segregation of brain tumor entails partition of tumor area, edema, necrosis, gray matter, white matter and cerebrospinal fluid. Accurate segmentation and cataloguing of aberrations are not up-front. Additional methodologies has to be employed exploited for accurate and efficient segmentation. Brain tumors are characterized based upon their degree of hostility. World Health Organization categorizes [20], [21] the brain tumor into four different grades, grade I – IV based on the severity of the tumor.

2.0 RELATED WORKS

A MRI brain tumor classification has been demonstrated [1] utilizing the neuro-fuzzy inference system. The system uses four abnormal brain tumor image classes such as metastases, meningioma, glioma and astrocytoma for its classification. Also, the artificial neural networks and fuzzy systems are analysed and compared with each other to show the dominance of ANFIS system. By combining conventional MRI and perfusion MR imaging, a computer based SVM classification system [2] is investigated and executed for different types of brain tumor for its classification. Histologically diagnosed 102 MRI brain tumor images were manipulated and it is observed that the developed system yields an accuracy of 85%, sensitivity of 87% and specificity of 79%.

A threefold diagnostic system [3] is proposed. Initially, the system significantly influences the brain glioma discrimination utilizing different Magnetic Resonance Spectroscopy scanners of 1.5 Tesla and 3 Tesla. Next the low, intermediate and high gliomas are classified and statistically evaluated based upon the discriminative potential of the metabolic markers. And finally, the diagnostic value of new metabolic ratios in the discrimination of complex glioma cases are examined. Clustering algorithms such as K-means, Self-Organizing Map, hierarchical clustering and fuzzy C-means were analysed [4] utilizing the MRI axial brain image to track the tumor area. Clustering algorithms were applied to the color image which is converted from the grayscale. By analysing the algorithms, it is noted that K-means and Hierarchical clustering achieved about 95% of efficiency when compared to other two algorithms. 275 benchmarked MRI brain images of size 256×256 is exploited through the developed automatic brain tumor classification system where 278 features are extracted. The automatic system incorporates neural network (NN) and K-Nearest Neighbor (K-NN) algorithms [5] for the tumor classification. The experimental results shows that the approach achieved 100% classification accuracy using K-NN and 98.92% using NN.

Four different brain tumor classes [6] such as Astrocytoma, Meningioma, Metastatic bronchogenic carcinoma, and Sarcoma were considered and utilized in the developed classification system. The Gray level Co-occurrence Matrix texture features were extracted for each class and given as input to the two-layered Feed forward Neural Network. And, it is observed that the developed system gave 97.5% classification rate. An appropriate method [7] for an effective denoise image from rician noise that assists the physicians is suggested and the prediction of Glioma in the MR images is proposed using weight optimized neural network. A three stage intelligent method for classifying the MRI brain tumor is proposed [8]. First the noise is removed and the contrast is enhanced as a pre-processing step. Secondly, the features from the pre-processed image is extracted and the dimensions of the feature data is reduced by Principal Component Analysis. The last step is performed to classify the brain images as normal, Edema, Cancer, or Not-classified using Back-Propagation Neural Network (BPNN) based-on Pearson correlation coefficient which gave an accuracy rate of 96.8%.

Characterization of brain tumor texture using a stochastic model [9] is proposed. A modified AdaBoost algorithm that assigns weights to the component classifiers is involved in the system to classify the difficult samples. The proposed method utilizes 300 MR images from 14 patients and compared with the BRATS2012 dataset to show its superiority. The pre-processing techniques on medical image data and few intelligent techniques for classification is reviewed. It is found and concluded that artificial neural network [10] is a promising technique for medical image data classification which gives higher percentage of accuracy. The possible abnormal tumor area in the MRI is extracted by using the morphological operations and the traditional level set technique [11]. The candidate tumor area is classified by using neurofuzzy and the evaluation results shows that the proposed method is more precise and robust for brain tumor segmentation in MR Images.

An automatic MRI brain tumor segmentation is proposed. Local independent projection-based classification [12] is used for the classifying each voxel into different classes. 80 brain tumor MRI images with ground truth data are used as training data and 40 images without ground truth data are used as testing data. The results obtained are compared with other state-of-art methodologies. An MRI brain classification system is performed [13] using energy coefficients and neural network. For performing classification, features are extracted based on the vector detail coefficients horizontal, vertical, diagonal and vector approximation of the wavelet decomposition at each level. Classification is performed to differentiate the types of normal brain disease, Alzheimer's disease, glioma and carcinoma. A semi-automated segmentation system for Glioblastoma Multiforme (GBM) feature detection is framed out [14] and the texture feature extraction from gray level co-occurrence matrix is presented. The classification results shows that out of 22 patients, an accuracy of 75.58 % is achieved for distinguishing GBM phenotypes using decision tree model. A brain tumor classification system using Probabilistic Neural Networks [15] is presented. The features of the MRI brain is extracted using principal component analysis. The brain tumor is classified differentiating normal, benign and malignant tumor parts.

3.0 OVERALL PROPOSED SYSTEM ARCHITECTURE

The proposed system involves various phases in which the system detects and classifies the MRI brain tumor images as benign and malignant.

The overall architecture of the proposed system is shown in Figure 1. The axial view of T1-weighted and T2-weighted images of MRI is manipulated in the process that is carried out. Image sharpening is performed over the T1-weighted image and the T2-weighted image is exploited using anisotropic diffusion filter. Alpha blending is used to blend both the MRI sequences where it is subjected to pass through the post-processing stage and the classification stage.
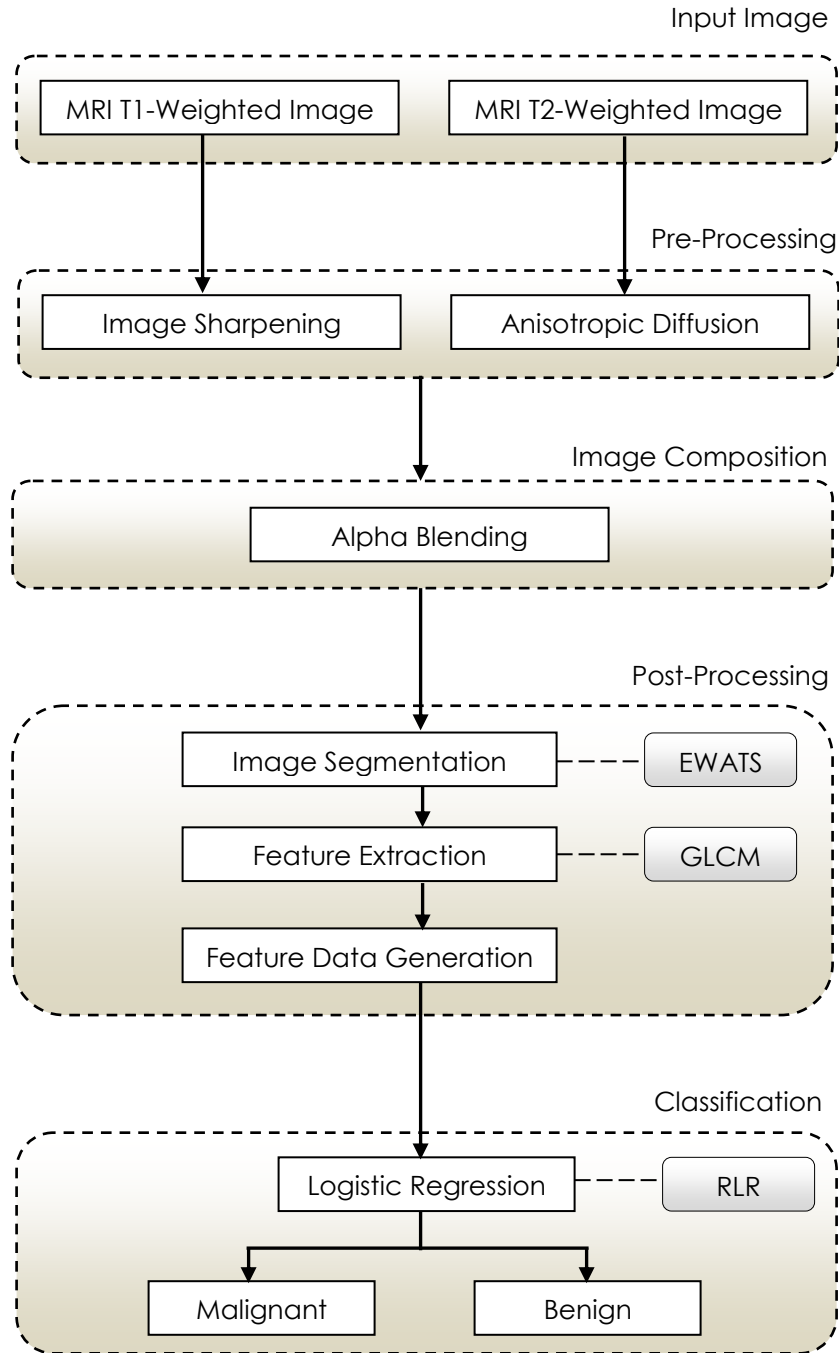
Figure 1 Overall architecture of the proposed System

3.1 Image Sharpening

The clarity of the T1-weighted image is described by its sharpness. An unsharp mask is used for attaining a sharp image. Additional information will not be created but it significantly improves the particulars of the edges in the image. The algorithm for image sharpening is given below.

$T1 \rightarrow Input\ Image$
$I_{hc} \rightarrow High\ Contrast\ Image$
$U_{msk} \rightarrow Unsharp\ Mask$
$Gb \rightarrow Gaussian\ Blur$
$Srp \rightarrow Sharpened\ Image$
$NSrp \rightarrow Normalized\ Sharpened\ Image$

Read T1-weighted image, $T1_i = \{T1_1, T1_2, \ldots \ldots T1_n\}$
{
　For (all images in $T1_i$)
　{
　　Create $U_{msk} \leftarrow Gb$;
　　Convert $T1$ to I_{hc} ;
　　$Srp = I_{hc} + U_{msk}$;
　　$NSrp = Srp + T1$;
　}
}

All the input T1-weighted images undergo the algorithmic steps to obtain a normalized sharpened output image where it appreciably improves the edges of the images.

3.2 Anisotropic Diffusion

Because the MRI data have low signal-to-noise ratios, the boundaries in the images will be obscured by the noise or their edges will be indistinguishable from other edges. The anisotropic diffusion filter [16] satisfy the main criteria of minimizing the information loss by preserving object boundaries and detailed structures, efficiently. It also removes the noise in the regions of homogeneous physical properties, and enhance the morphological definition by sharpening the discontinuities.

By reflecting the anisotropic diffusion equation as D_p,

$$D_p = div(c(m,n,p)\nabla D) \qquad (1)$$

$$= c(m,n,p)\nabla^2 D + \nabla_c \cdot \nabla D \qquad (2)$$

where, (m,n) is the spatial location in the image, ∇^2 and ∇ are the depiction of the Laplacian and gradient operators pertaining the spatial variables and the indication of the divergence operator. The diffusion coefficient function variable, c contrasts with the monotonic declining of the image gradient. If the variable c is a constant value, then the outcome of D_p which is the isotropic heat diffusion, convolves with a Gaussian kernel with the variance. The Gaussian kernel surges linearly with time.

This convolution between the isotropic diffusion and the Gaussian kernel with variance blurs both resilient and weak edges. The diffusion coefficient function is expressed as

$$c(m,n,p) = e^{\frac{-\|\nabla(m,n,p)\|^2}{2q^2}} \qquad (3)$$

which honours the high contrast edges when compared to low contrast edges. The parameter q is the gradient modulus threshold that regulates the transference.

3.3 Image Composition

The process of combining an image with other image to create a new blended image manipulating the translucency is known as alpha blending [19] or in general image compositing. Here, the pre-processed T1-weighted and T2-weighted images are composited to achieve an improved blended image. This improved blended MR image is further send to the next stage for segmenting the tumor area.
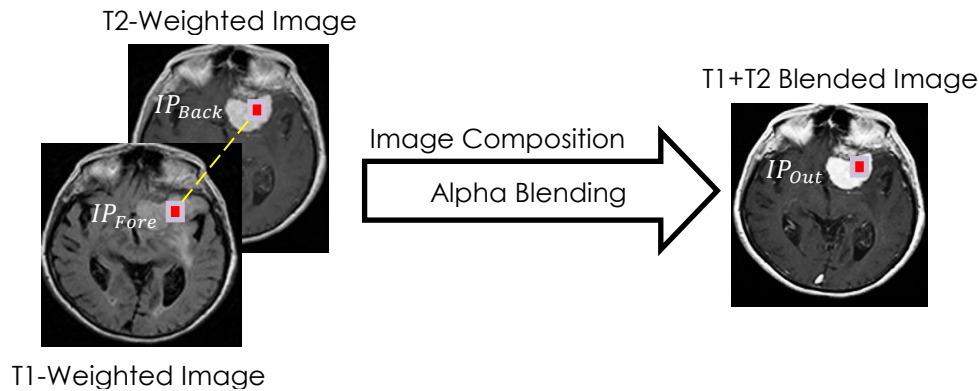

Figure 2 Image composition of T1-weighted and T2-weighted MR images

In image compositing, assume that the foreground image pixel (IP_{Fore}) is place above the background image pixel (IP_{Back}), then the output, IP_0 is given as

$$IP_0 = \alpha * IP_{Fore} + (1 - \alpha) * IP_{Back} \qquad (4)$$

The output of the intensity image, I_0 is the weighted sum of the foreground image intensity I_{Fore} and the background image intensity, I_{Back}. The parameter, α decides the ratio of translucency between the two images. The value of α will be decided between 0 and 1. When α is 0, it is completely transparent and when α is 1, it is completely opaque.

3.4 EWATS: Enhanced Watershed Segmentation

Watershed segmentation is a predominant segmentation scheme with several advantages. It ensures the closed region boundaries and gives solid results. It is a way of automatically separating or making regions distinct without touching. The watershed algorithm uses concepts from mathematical morphological operations to partition images into homogeneous regions. To improve the conventional watershed model, the proposed enhanced model uses a multiscale morphological gradient to calculate the intensity of the image. These values are multiplied and markers are extracted from this composite gradient image using a thresholding technique.

On deeper analysis, it was found that over segmentation problem can sometimes be solved by the correct usage of the threshold value. The over segmentation result shows that the selection of threshold is very important. Choosing a very low value results in important regions merged together and a high value results in numerous number of small regions, resulting in over segmentation. The over segmentation problem can be solved by using an optimal threshold value. A method to automatically calculate this optimal threshold value was used. The optimal threshold value was computed using minimal projection distance.

Assume that the image f is an element of the space K(D) of a connected domain D then the topographical distance between points m and n in D is given in equation (5).

$$I_f(m,n) = in_\gamma \int \|\nabla f(\gamma(s))\| \, ds \qquad (5)$$

where, 'in$_\gamma$ ' is over all paths (smooth curve) inside D , defines the watershed as follows. Let f $\in$K(D) have a minima$\{m_k\}_{k\in I}$, for some index set I. The catchment basin KB (m$_i$) of a minimum m$_i$ is defined as the set of points K$\in$ D, which are topographically closer to m$_i$ than to any other regional minimum m$_j$. The enhanced watershed segmentation algorithm is mentioned below.

Step 1: *Read gray scale image as input*
Step 2: *Apply morphological operation opening to the enhanced image*
Step 3: *Apply Sobel operator for edge detection and find the gradient magnitude.*

Step 4: *Apply watershed segmentation with markers into ROI and background.*
Step 5: *Calculate regional maxima of the reconstructed image.*

The Sobel filter finds the approximate absolute gradient magnitudes at each location of an image and accomplishes a 2-D spatial gradient magnitude that highlights the high spatial frequency regions. The matlab function, imregionalmax is employed to find the regional maxima which is more suitable to find the bright edges.

3.5 Feature Extraction

Texture features are extracted from the segmented image using GLCM techniques. Features are the characteristics of the objects of interest. It is the illustrative of the maximum pertinent facts that the image has to offer for a comprehensive characterization of a lesion. Feature extraction approaches analyse the various objects in the image and the image itself to extract the most prominent features to classify the objects. The first order and the second order features are extracted. The first order features extracted are Mean, Variance, Standard Deviation, Skewness and Kurtosis. The extracted second order features are Contrast, Correlation, Energy, Homogeneity, Smoothness and Eccentricity.

3.5.1 Feature Dataset Generation

In this experimental work, 53 T1-weighted MR images and its respective 53 T2-weighted MR images were investigated. Since this work is focused towards 2D, the axial view of both T1-weighted and T2-weighted MR images are considered and manipulated to extract the feature dataset. The size of all the images that are processed were 256*256 with 300 dpi. All the 106 MR images are processed to extract the first order and second order features which in turn be classified. The datasets were obtained from Government General Hospital, Puducherry, India (http://www.mypacs.net/). Christian Medical College, Vellore, India and Devi Scans, Thiruvananthapuram, India.

3.5.2 Regularized Logistic Regression (RLR)

One of the most popular algorithms in the field of machine learning is the concept of logistic regression [17]. As the name suggests it isn't a regression algorithm, instead is a classification algorithm. To perform the logistic regression first all the values are passed through the sigmoid function so that the output lies in the range of 0 and 1, and the cost function graph should be in a hyperbolic shape so that a minimum can be generated. The sigmoid function is given as:

$$L_\theta(x) = s(\theta^T x) \qquad (6)$$

Here the L$_\theta$ value is the values that are to be generate, and is the function which classifies the result and s is the sigmoid function, and can be given as:

$$s(z) = \frac{1}{1+e^{-z}} \qquad (7)$$

Cost Function

The cost function is calculated to find the parameter set θ in order to classify the result. The cost function is given as:

$$C(\theta) = \frac{1}{n}\sum_{i=1}^{n}\left[-y^{(i)}\log\left(L_\theta(x^{(i)})\right) - (1-y^{(i)})\log\left(1 - L_\theta(x^{(i)})\right)\right] \qquad (8)$$

If there is a large number of features for a moderate amount of dataset, the function overfits the data. As a result of overfitting, the prediction becomes very difficult. Consequently, in order to prevent the overfitting the data we apply regularization. Here the parameter, λ is to be selected based on the accuracy of the prediction made by the algorithm. Cost function with regularization can be given as:

$$C(\theta) = \frac{1}{n}\sum_{i=1}^{n}\left[-y^{(i)}\log\left(L_\theta(x^{(i)})\right)\right.$$
$$\left. - (1-y^{(i)})\log\left(1 - L_\theta(x^{(i)})\right)\right] + \frac{\lambda}{n}\theta_j$$
$$for\ j \geq 1 \qquad (9)$$

Gradient Function

Once the cost function $C(\theta)$ is defined, the minima value has to be found out by the gradient function. The gradient function to find the minima value is given by

$$\frac{\partial C}{\partial \theta_j} = \frac{1}{n}\sum_{i=1}^{n}((L_\theta(x^{(i)}) - y^{(i)})x_j^{(i)}) \qquad (10)$$

As the regularization parameter is applied for the cost function, it is also applied to the gradient function. Therefore, the following equations are got.

4.0 RESULTS AND DISCUSSIONS

$$\frac{\partial C(\theta)}{\partial \theta_0} = \frac{1}{n}\sum_{i=1}^{n}((L_\theta(x^{(i)}) - y^{(i)})x_j^{(i)}) \quad for\ j = 0 \quad (11)$$

$$\frac{\partial C(\theta)}{\partial \theta_j} = \frac{1}{n}\sum_{i=1}^{n}((L_\theta(x^{(i)}) - y^{(i)})x_j^{(i)}) + \frac{\lambda}{n}\theta_j \quad for\ j \geq 1 \quad (12)$$

Here, the regularization parameter is not applied to the parameter θ, since the initial value does not affect the process.

Now, once the cost function and the descent matrices are calculated, the gradient descent is applied to find the minimum value. The gradient descent calculation can be performed by the following equation.

$$\theta_j := \theta_j - \alpha\frac{1}{n}\sum_{i=1}^{n}((L_\theta(x^{(i)}) - y^{(i)})x_j^{(i)}) \qquad (13)$$
$$(simultaneously\ update\ \theta_j\ for\ all\ j).$$

Here, the matlab function, fminunc can be utilized instead of the gradient descent function since it is more efficient in handling large set of parameters.
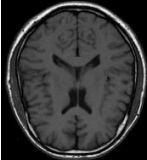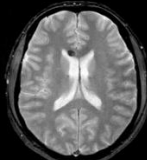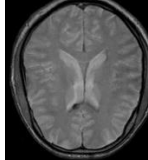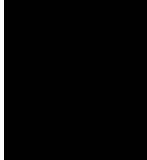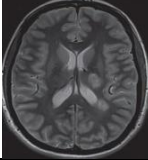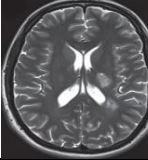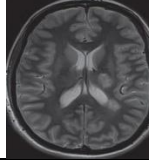
Now, L_θ is calculated for the new set of values and the probability of tumor presence is generated.

For instance, empirically 0.5 is applied as the probability factor to classify the tumor in the MR images. Hence,

$$L_\theta = \begin{cases} +ve, benign; & L_\theta \geq 0.5 \\ -ve, malignant; & L_\theta < 0.5 \end{cases} \qquad (14)$$

If the accuracy of the classification needs to be more stringent, then the empirical threshold value of 0.5 can be increased.
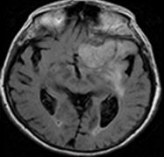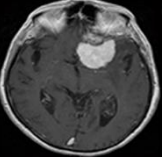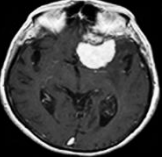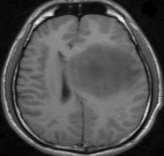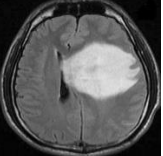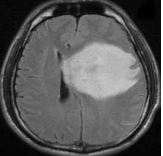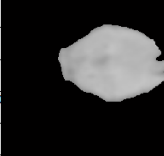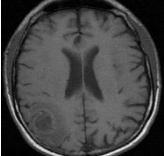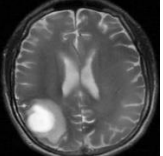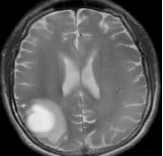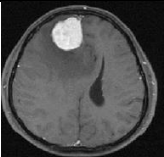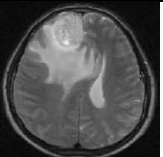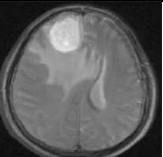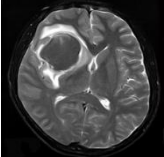
Table 1 MR Image sequence (Non-Tumor) – Ground Truth Segmented Image Vs Proposed Segmented Image

Sl. No	T1-Weighted Image	T2-Weighted Image	Blended Image	Ground Truth Image	Proposed Segmented Image
1					
2					

Two datasets of MR Image sequence with no tumor is shown above in a tabular form. Since there is no tumor in the given input images, the segmented output images also show no trace of tumor where the output image is blank.

Table 2 MR Image sequence (Tumor) – Ground Truth Segmented Image Vs Proposed Segmented Image

Sl. No	T1-Weighted Image	T2-Weighted Image	Blended Image	Ground Truth Image	Proposed Tumor Segmented Image
1					
2					
3					
4					
5					

MR Image sequence with no presence of tumor is shown above in a tabular form. It is visibly evident that the proposed extracted tumor part from the images is almost similar to that of the ground truth image. This shows that the segmentation algorithm, EWATS works competently to attain the tumor part.

4.1 Extracted Feature Dataset

Table 3 signifies the first order features from the proposed extracted data. The first order image features are extracted for five input MR Images. The first image has the highest kurtosis value and the third image has the lowest kurtosis value. The fourth image has highest skewness and the third image has the least skewness.
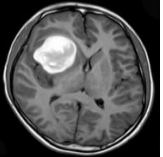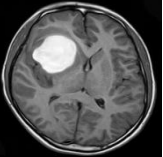
Table 3 Proposed Extracted Data – First Order Features

Image	Mean	Variance	SD	Skewness	Kurtosis
1	0.0491	0.0467	0.2161	4.1726	18.4105
2	0.1132	0.1004	0.3168	2.4415	6.9611
3	0.2136	0.4098	0.4098	1.3979	2.9540
4	0.0509	0.0484	0.0484	4.0842	17.6808
5	0.0830	0.0761	0.2759	3.0235	10.1418

Table 4 indicates the second order features from the proposed extracted data. The second order image features are extracted for five input MR images. The third image has the highest energy and the second image has the lowest energy. The third image has highest contrast and the fifth image has the least contrast. Highest smoothness value is obtained from the third image and the least smoothness is with the first image.

Table 4 Proposed Extracted Data –Second Order Features

Images	Contrast	Correlation	Energy	Homogeneity	Smoothness	Eccentricity
1	1.0971	0.1376	3.1066	0.0104	0.0446	0.7153
2	2.0718	0.1366	1.3479	0.0075	0.0912	0.5465
3	6.1762	0.0419	7.1449	0.0468	0.1438	0.6780
4	4.9188	0.0738	2.9949	0.0175	0.0461	0.4314
5	1.0573	0.1067	1.8389	0.0765	0.0707	0.5404

Table 5 signifies the quality metrics for the proposed extracted data. The quality metrics for the proposed extracted five image data is provided in the above table. All the five input images achieved almost the maximum possible structural content with slight variation from the ground truth data. The second image achieved the maximum structural content whereas the third image has the least structural content. The highest normalized absolute error is with the first image and the lowest normalized absolute error is with the fourth image.

Table 5 Proposed Extracted Data - Quality Metrics

Image	PSNR	Structural Similarity	Normalized Cross-Correlation	Normalized Absolute Error
1	22.8312	0.9812	0.9342	0.1214
2	21.6234	0.9985	0.9682	0.0772
3	24.3574	0.9321	0.9462	0.1013
4	26.9351	0.9989	0.9585	0.0205
5	28.5131	0.9811	0.9391	0.1030

Table 6 signifies the quality metrics for the ground truth dataset. The quality metrics for the five ground truth image data is provided in the above table. All the five input images achieved almost the maximum possible structural content. The second image achieved the maximum structural content whereas the third image has the least structural content. The highest normalized absolute error is with the third image and the lowest normalized absolute error is with the second image. It is observed that the difference between the ground truth data and the proposed extracted data is very minimal.

Table 6 Ground Truth Dataset – Quality Metrics

Image	PSNR	Structural Similarity	Normalized Cross-Correlation	Normalized Absolute Error
1	22.3113	0.9702	0.9241	0.1223
2	21.2034	0.9882	0.9412	0.0942
3	23.1554	0.9422	0.9160	0.1843
4	26.4150	0.9872	0.8995	0.1201
5	27.3201	0.9731	0.9142	0.1110

4.2 Classification Efficiency

The achieved efficiency of different segmentation methods along with the classification methods are tabulated. Three other methodologies are compared with the proposed methodology and it is interesting to note that the proposed system has the upper hand over the other three different methodologies. The efficiency is calculated based upon its sensitivity, specificity and accuracy.

Table 7 Classification efficiency of different methodologies compared to the proposed method

Methods	TP	TN	FP	FN	Sensitivity (%)	Specificity (%)	Accuracy (%)
MOR + SVM	20	12	10	8	71	54	64
WS + SVM	30	10	5	5	85	66	80
EWATS+SVM	42	5	2	1	97	71	94
EWATS + RLR (Proposed Method)	42	6	1	1	97	86	96

MOR – Morphology; WS – Watershed Segmentation; SVM – Support Vector Machine; EWS – Enhanced Watershed Segmentation; RLR – Regularized Logistic Regression.

The efficiency rate of the various classification algorithm is represented in the Table 7. It is observed that the combined techniques of MOR+SVM gave the least accuracy of 64% and interestingly the proposed methodology, EWATS+RLR the attained maximum accuracy rate of 96% when compared to other hybrid techniques.

The visual representation of the quality metrics between the ground truth data and the achieved data is shown below in graphs.
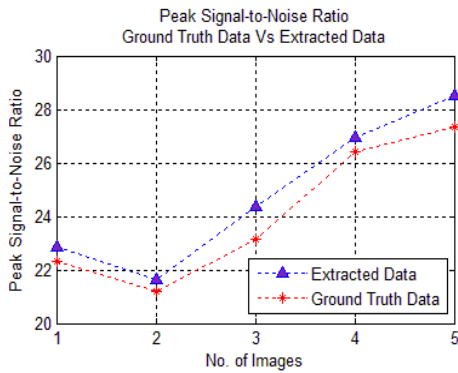

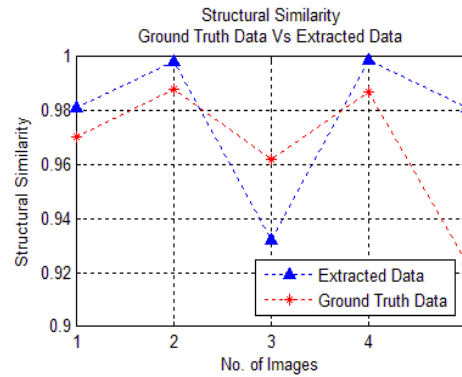**Figure 3** PSNR Ground Truth Vs Achieved Data

Figure 4 SS Ground Truth Vs Achieved Data

Figure 3 graphically illustrates the peak signal-to-noise ratio of the ground truth data and the extracted data from the proposed methodology. Figure 4 illustrates graphically the structural similarity between the ground truth images and the extracted data from the proposed methodology.
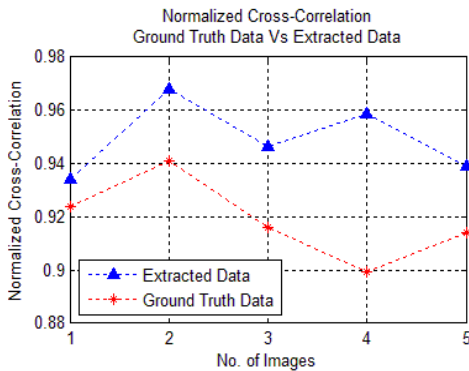

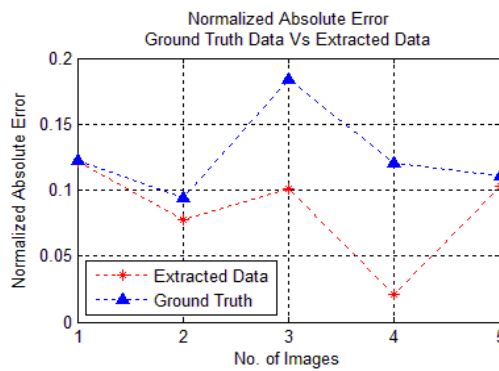**Figure 5** NCC Ground Truth Vs Achieved Data

Figure 6 NAE Ground Truth Vs Achieved Data

Figure 5 graphically illustrates the normalized cross-correlation of the ground truth data and the achieved data from the proposed methodology. Figure 6 illustrates graphically the normalized absolute error between the ground truth images and the achieved data from the proposed methodology.

The relationship between the maximum probable value of a signal and the power of distorting noise that affects the quality of its representation is provided by Peak Signal-to-Noise Ratio (PSNR). Structural Similarity (SS) measures the structural likeliness by comparing the input images and the processed images pertaining to the

flawless quality. Normalized cross-correlation (NCC) delineates the way of registering and aligning images by translation. Normalized absolute error (NAE) calculates the amount of modified decompressed image pertaining to its original one. Therefore, higher value of normalized absolute error implies lower quality.
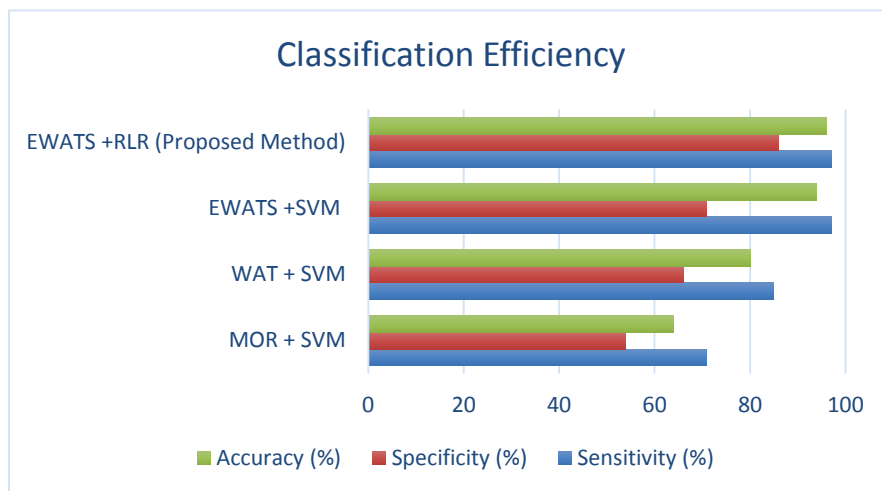

Figure 7 Comparison of Classification Efficiency between Proposed Method and Other methods

The comparison between various hybrid techniques are presented in the above displayed graph, Figure 7. It is interestingly noted that the proposed methodology, WATS+ RLR was able to achieve 96% of accuracy, 86 % of specificity and 97% of sensitivity when executed.

5.0 CONCLUSION

An efficient computer based diagnostic system for detecting and classifying the MRI brain tumor is proposed and implemented. The diagnostic system utilizes a multi-fold phases for the final execution. The first order and the second order features of the images are extracted efficiently and also the quality metrics are performed. All the output that is obtained are compared with the ground truth dataset. By the comparison, it is well understood that the attained output is superior to the ground truth data. The developed diagnostic system was able to attain an efficiency rate of 96 % in classifying whether the brain tumor is benign or malignant.

References

[1]   ] D. Jude Hemanth, C.Kezi Selva Vijila and J.Anitha. 2010. Application of Neuro-Fuzzy Model for MR Brain Tumor Image Classification. International Journal of Biomedical Soft Computing and Human Sciences. 16(1): 95-102.
[2]   Evangelia I. Zacharaki, Sumei Wang, Sanjeev Chawla, Dong Soo Yoo, Ronald Wolf, Elias R. Melhem, and Christos Davatzikos. 2010. Classification of brain tumor type and grade using MRI texture and shape in a machine learning scheme. Magn. Reson. Med. 62(6):1609–1618.
[3]   M.G.Kounelakis, I.N.Dimou, M.E.Zervakis, I.Tsougos, E.Tsolaki, E.Kousi, E.Kapsalaki, and K.Theodorou. 2011. Strengths and Weaknesses of 1.5T and 3T MRS Data in Brain Glioma Classification. IEEE Transactions on Information Technology in Biomedicine. 15(4): 647-654.
[4]   P. Tamije Selvy, V. Palanisamy, T. Purusothaman. 2011. Performance Analysis of Clustering Algorithms in Brain Tumor Detection of MR Images. European Journal of Scientific Research. Euro Journals Publishing. 62(3): 321-330.
[5]   Amer Al-Badarneh, Hassan Najadat and Ali M. Alraziqi. A Classifier to Detect Tumor Disease in MRI Brain Images. IEEE/ACM International Conference on Advances in Social Networks Analysis and Mining (ASONAM), 2012, Istanbul. 26-29 August 2012. 784-787.
[6]   Nitish Zulpe and Vrushsen Pawar. 2012. GLCM Textural Features for Brain Tumor Classification. International Journal of Computer Science Issues. 9(3): 354-359.
[7]   S. Karpagam and S. Gowri. 2013. Development of an Optimized Glioma Prediction Technique Using Genetic Algorithm Based Neural Network. Middle-East Journal of Scientific Research. 16(2): 210-220.
[8]   Magdi B. M. Amien, Ahmed Abd-elrehman, Walla Ibrahim. 2013. An Intelligent-Model for Automatic Brain-Tumor Diagnosis based-on MRI Images. International Journal of Computer Applications. 72(23): 21-24.
[9]   AtiqIslam, Syed M.S.Reza, and Khan M.Iftekharuddin. 2013. Multifractal Texture Estimation for Detection and Segmentation of Brain Tumors. IEEE Transactions on Biomedical Engineering. 60(11): 3204-3215.
[10]   Hota H.S., Shukla S.P. and Gulhare Kajal Kiran. 2013. Review of Intelligent Techniques Applied for Classification and Preprocessing of Medical Image Data. International Journal of Computer Science Issues. 10(3): 267-272.
[11]   Mohammad. V. Malakooti, Seyed Ali Mousavi, and Navid Hashemi Taba. 2013. MRI Brain Image Segmentation Using Combined Fuzzy Logic and Neural Networks for Tumor Detection. Journal of Academic and Applied Studies. 3(5):1-15.

[12] Meiyan Huang, Wei Yang, Yao Wu, Jun Jiang, Wufan Chen. 2014. Brain Tumor Segmentation Based on Local Independent Projection-Based Classification. IEEE Transactions on Biomedical Engineering. 61(10): 2633-2644.

[13] Auli Damayanti and Indah Werdiningsih. 2014. Classification of Magnetic Resonance (MR) Brain Images Using Energy Coefficient and Neural Network. Applied Mathematical Sciences. 8(11): 517 - 524.

[14] Ahmad Chaddad, Pascal O. Zinn and Rivka R. Colen. Radiomics Texture Feature Extraction for Characterizing GBM Phenotypes using GLCM. IEEE 12th International Symposium on Biomedical Imaging (ISBI), 2015, Neyork, NY. 16-19 April 2015. 84-87**.**

[15] Sonali B. Gaikwad, and Madhuri S. Joshi. 2015. Brain Tumor Classification using Principal Component Analysis and Probabilistic Neural Network. International Journal of Computer Applications. 120(3): 5-9.

[16] Jingjing Gao, Mei Xie. 2009. Skull-stripping MR Brain Images Using Anisotropic Diffusion Filtering and Morphological Processing. IEEE International Symposium on Computer Network and Multimedia Technology Conference (CNMT), 2009, Wuhan, China. 18-20 January 2009. 1-4.

[17] Viv Bewick, Liz Cheek, Jonathan Ball. 2005. Statistics review: Logistic regression. Critical Care, BioMed Central Ltd. 9(1): 112-118.

[18] Stefan Bauer, Roland Wiest, Lutz-P Nolte and Maurici Reyes. 2013. A survey of MR-based medical image analysis for brain tumor studies. Phy. Med. Biol. IOP Publishing. 58: 97-129.

[19] A. Guidi, R. Achanta, C. Fredembach e S. Susstrunk. GUI-Aided NIR and Color Image Blending. MELECON 2010 - 15th IEEE Mediterranean Electro technical Conference, 2010, Valletta. 26-28 April 2010. 1111 -1116.

[20] David N. Louis. Hiroko Ohgaki. Otmar D. Wiestler. Webster K. Cavenee. Peter C. Burger. Anne Jouvet. Bernd W. Scheithauer. Paul Kleihues. 2007. The 2007 WHO Classification of Tumours of the Central Nervous System. Acta Neuropathologica. Springer-Verlag. 114(2): 97-109.

[21] Kraig Moore and Lyndon Kim. 2010. Primary Brain Tumors: Characteristics, Practical Diagnostic and Treatment Approaches. In S.K.Ray(ed). Glioblastoma: Molecular Mechanisms of Pathogenesis and Current Therapeutic Strategies. Springer Science + Business Media.